INSTITUT DE FRANCE
Académie des sciences

Comptes Rendus

Mécanique

Naima Benmakhlouf, Soufien Azzouz, Lamine Hassini and Afif El Cafsi

2D model simulating the hydro-rheological behavior of leather during convective drying

Volume 349, issue 2 (2021), p. 305-322

Published online: 7 June 2021

https://doi.org/10.5802/crmeca.86

Les Comptes Rendus. Mécanique *sont membres du Centre Mersenne pour l'édition scientifique ouverte*
www.centre-mersenne.org
e-ISSN : 1873-7234

Comptes Rendus
Mécanique
2021, 349, nº 2, p. 305-322
https://doi.org/10.5802/crmeca.86

Synthese / *Synthèse*

2D model simulating the hydro-rheological behavior of leather during convective drying

Naima Benmakhlouf[*, a, b], Soufien Azzouz[a], Lamine Hassini[a, c] and Afif El Cafsi[a]

[a] University of Tunis El Manar, Faculté des Sciences de Tunis, Laboratoire d'Energétique et des Transferts Thermique et Massique (LETTM), University Campus, 2092 El Manar II, Tunis, Tunisia

[b] Al-Bahaha University, Qilwah college of Science & Arts, Physics Department, Saudi Arabia

[c] Shaqra University, College of Science and Humanities - Al Quwaiiyah, Department of Physics, Saudi Arabia

E-mails: benmakhlouf.naima@yahoo.fr (N. Benmakhlouf), azsoufien@yahoo.fr (S. Azzouz), hassini_lamine@yahoo.fr (L. Hassini), afifkafsi@yahoo.fr (A. El Cafsi)

Abstract. An experimental and numerical study of a two-dimensional spatio-temporal variation of the temperature, moisture content, and mechanical stress during the convective drying process of unsaturated and deformable products (leather) were conducted. The bovine leather sample response under convective drying is described by a mathematical model. The leather sample was modeled by an elastic medium, and the mass, heat, and momentum transfer principles are applied. The numerical results agreed well with the corresponding experimental data. The variation of the internal temperature and moisture content was simulated for different drying conditions. A reduction by 15 °C was noted in the optimum temperature for best product quality when the drying air relative humidity was 20%. The cost to achieve a better quality product was found to be minimized due to the decrease in the optimum temperature. The presented simulation results of the elastic material could be applied to the leather, which will reduce the needed time of exposure for predetermined final water content. The damage of the sample is more likely to occur at the beginning of the drying in the time interval of 300–400 s. According to these simulations, the sample's face, which is exposed to the drying air, has the highest stress; therefore, the sample's face is at a high risk of cracking. It is also observed that the risk of damage to the sample corresponding to the maximum level of the stress is higher for the highest drying temperature of 60 °C. The peak of the three thicknesses of leather can be achieved for normal stresses in the interval of 60,000 to 140,000 MPa at around 10,000 s.

Keywords. Viscoelastic material, Leather, Moisture content, Convective drying, Kinetics, Simulation, Rheological behavior.

Manuscript received 18th February 2021, revised 9th April 2021 and 3rd May 2021, accepted 4th May 2021.

[*] Corresponding author.

1. Introduction

The main factors affecting the drying processes are the nature and the desired functionality of the dried product, and the quantity of the removed water. Convective drying is considered the most common and popular drying mode. During the convective drying, the heat is transferred to the product from the drying, while mass is transferred from the core of the product to its surface and then to the surroundings. The main purpose of drying is to stabilize the product, to bring it to the recommended final moisture for long-term use and storage and to improve its quality. Improving the quality of leather requires the mastery of drying techniques that are delicate and expensive on an industrial scale. Industrial drying, with all the inherent operations, is very energy-intensive. The complexity involved in the drying process is the coupling of heat and mass transfer in the dried product. Mathematical models that describe the physical phenomena were developed to predict heat transfer and mass concentration in the dried product. Multimode-coupled heat and mass transfer models simulated water vapor and liquid diffusion and convection. The product's shrinkage because of water loss by evaporation was not considered by researchers [1–3]. However, some works considered the shrinkage effect without determining the mechanical stresses [4–6]. The control of dried product's quality is highly affected by the product deformation. Ketelaars *et al.* [7] proposed a two-dimensional (2D) convective drying model for the drying stresses and studied linear and plane stresses. The authors confirmed the absence of any stresses at the beginning of the process because of low Young's modulus values. The development of stresses was appeared after a few hours of the start of the process due to the decrease in the material moisture content and the presence of moisture concentration gradients. Hawlader [8] developed a mathematical model to simulate heat and mass transfer in products that could have shrinkage during the drying process. Numerical techniques are used to solve simultaneously the governing heat and mass transfer equations. A heat pump dryer was used to conduct experiments to validate the model. Several samples were placed in the dryer and, after the commencement of each drying test, one sample was taken out at a regular time interval. The bone-dry mass of each piece was also determined to evaluate the moisture distribution within the materials. Perré [9] used a finite element method to describe the shape of porous material that largely deforms because of shrinkage phenomena. Some mathematical modeling neglected the effect of shrinkage to simplify the governing equations. This approach was approved to be appropriate for products with a very small shrinkage factor. Other researchers studied shrinkage deformation theoretically by mathematical modeling of heat and mass transfer processes and experimentally on some fruits and vegetables. It was concluded that the critical moisture content was not the same as that used in published literature [10, 11]. Numerical solutions of the mass transfer in the drying liquid at an equilibrium state was developed by Silva, Precker, [12]. The diffusive and capillary porous models have widely used modeling approaches in the literature. The diffusive approach assumes the solid and liquid phases as a homogeneous material described by Fick's law [13–15]. The approach of the capillary porous model considers the solid and liquid phases, and the momentum equation is used to obtain the solid displacement [16–18]. The product's moisture movement is affected by capillary forces, osmotic pressure, gravitation, and thermo-diffusion [19, 20]. A spherical mathematical model was developed to study the kinetics of drying in a thin layer of grape seeds [21]. The convective and equilibrium boundary conditions were implemented and the results were compared to experimental data. The authors found that convective boundary conditions were in better agreement than the equilibrium conditions with the experimental results. Several drying methods have been studied for leather drying, and the most common were convective, vacuum, and microwaves drying [22]. The obtained results showed advantages in the improvement of the area yield. Using a statistical experimental design, regression models were formulated to describe how drying variables affect mechanical properties and area yield of chrome-free leather tanned

with glutaraldehyde. An effort was also made to estimate the effects of conditioning, staking, and drum milling on the area retention gained by toggle stretching. Drying leather by microwave was studied, and the obtained results showed advantages of utilizing microwave in the soft-leather drying. The results indicated that microwave drying would not damage leather collagen structure. Meanwhile, as microwave drying was even and would promote the combinations of collagen with other chemicals, the softness and mechanical properties of microwave dried leather were improved [23]. Historical leather and modern collagen-based material were studied by nuclear magnetic resonance (NMR) spectroscopy with a special focus on collagen gelatinization by Noemi Proietti [24].

Ershad-Langroudia *et al.* [25] have assessed the viscoelastic behavior of treated historical leather using nanocomposite by dynamic mechanical analysis. However, the works published by some others considered that leather is an elastic material [26]. On the other hand, some scientific works, dealing with the hydrothermal parameters of leather, considered that this material remains saturated over a large part of drying [27–29].

This present work a 2D transitory model describing the physical phenomena occurring inside deformable materials during the drying process. This model was applied to a saturated leather material. It was based on the Terzaghi theory of effective stress [30]. The particularity of the model is that it takes into account the strong coupling between mass transport and mechanical behavior through the solid deformation velocity and the liquid-phase pressure.

The hydrothermal part of the model is represented by the equations of diffusion/convection of liquid water and the heat conduction/convection coupled with the solid contraction velocity to describe the effect of shrinkage. The mechanical part of the model is based on Hooke's law in-plane strain with isotropic water shrinkage. Hence, the convective-type boundary conditions for the hydrothermal model and zero external stress for the mechanical model are imposed on the moving boundaries. The model is powered by the thermophysical properties determined from characterization experiments independent of the drying operation and performed on parallelepiped samples of the leather.

The governing equations with the boundary conditions have been numerically solved using the COMSOL "Multiphysics" software. The simulation results were validated based on experimental data. A vertical type tunnel with operating conditions controller was used as the experimental setup.

2. Material and experimental methods

2.1. *Preparation of leather samples*

The leather samples used in the present experiment were delivered by a Factory located in the Grombalia region at the Nabeul governorate in Tunisia. The samples were chrome-tanned hides collected from the industry just before the drying process. The leather samples' thickness is 2 mm, and the rectangular area of the cut leather is 0.16×0.14 m^2. Initially, the samples' moisture content is in the range of (50–53)%.

2.2. *Drying experiments*

The overall layout of the dryer is shown in Figure 1. It is a closed-loop wind tunnel with a horizontal grate. The experiments were conducted in a commonly used range of velocity, temperature, and relative humidity in the processes of convective drying. A fan of 2.5 kW capacity was used to generate the airflow, which is used to increase the heating coil's temperature. The homogenization of the air was ensured by a honeycomb filter. In the test section, the air flows are conducted

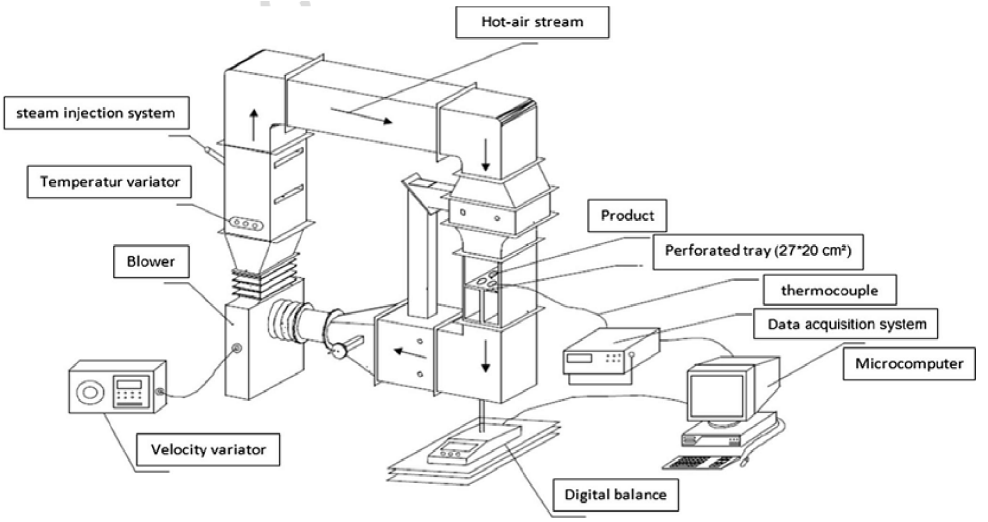

Figure 1. Schematic diagram of the convective dryer.

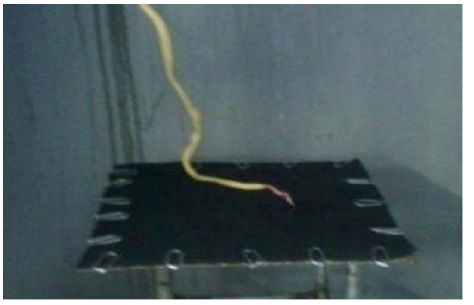

Figure 2. Orientation of the leather sample in the drying chamber.

perpendicularly to the dried product's surface to ensure optimal contact of the air-product and achieve higher heat transfer coefficients. A programmable controller is used to continuously control the temperature, velocity, and humidity.

The Tannery Megisserie du Maghreb (TMM) provided the crust leather used in the experiment. The used leather samples are maintained at low temperatures to avoid material degradation [31–36]. The product temperature and moisture content were measured and recorded by a data acquisition system.

The pieces were placed on a grid by fixing the flesh side to the surface of the grid, as shown in Figure 2. The experimental design with three variables; relative humidity, temperature, and the drying air velocity is considered. A thermocouple is used to measure the temperature inside the leather.

Electronic balance is used to continuously measure the product's weight loss for the entire product-support plate, and the measurements are recorded by the data acquisition and processing system.

A time interval of two minutes is adopted to measure the product's weight loss during the convective drying process. The relative humidity set point at which the process is terminated is taken according to the industry recommendation at 12%. The range of the operating and test

Table 1. Operating drying air conditions

Experiment	Temperature (°C)	Relative humidity (%)	Velocity of air ($m{\cdot}s^{-1}$)
1	40	20	1
2	45	20	1
3	50	20	1
4	55	20	1
5	60	20	1
6	50	20	1.5
7	50	20	2
8	50	30	1
9	50	45	1

conditions of the experiments was (40–60) °C for the temperature, (1–2) $m{\cdot}s^{-1}$ for the airspeed, and (20–45)% for the relative humidity. In every drying experiment, a cutting leather of mass of approximately 50 g was used. Each experiment was done at least twice in order to check the reproducibility of the drying curves. A vacuum oven at 104 °C for 24 h is used to determine the sample's dry mass at the end of every experiment. The conditions of the drying air are presented in Table 1.

Data analysis will be performed using variables which are given by the following equations

$$X(\%) = \left(\frac{M - M_d}{M}\right) \times 100, \tag{1}$$

where X—the content of moisture, M—the final product's mass, and M_d—the product's dried mass.

3. Mathematical modeling

The theory of averaging is widely used by authors working in mass and heat transfer in porous media Whitaker [37], Sandoval-Torres [38], Jomaa [39]. Whitaker's theory based on the method of volume averaging was generally used to predict heat and mass transfer in porous medium. This theory is based also on the conditions which require that the radius R_0 of the representative elementary volume is very small compared to the size of the medium to be dried and much larger than the characteristic dimension of the porosity. R_0 is between 10^{-1} m and 10^{-7} m (Gustavo [40], Collignon [41]).

The averaged equations involve measurable macroscopic quantities. For each phase, the energy transport, mass, and microscopic momentum equations generally have the form found in (2) for the studied variable G. The term J describes the diffusive flux of heat or mass. The term source under the action of a chemical reaction or a force is described by Φ.

$$\frac{\partial G_i}{\partial t} + \vec{\nabla}(G_i \vec{V}_i) = \vec{\nabla} \cdot J_i + \Phi_i. \tag{2}$$

By integrating (2) over the representative elementary volume (REV), based on the assumption that the REV is always fixed around a point and using the averaging theorem, the general form of the averaged transport equation is

$$\frac{\partial \langle G_i \rangle}{\partial t} + \vec{\nabla} \cdot \varepsilon_i \langle G \rangle^i \langle \vec{V}_i \rangle^i = \vec{\nabla} \cdot \langle G_i \rangle + \langle \Phi_i \rangle. \tag{3}$$

The equations of transport that bring us back to an average must be supplemented by constitutive relations, which make it possible to describe the interactions between the phases and the morphological properties.

3.1. *Mass transfer equations*

In the conservation of mass equation in two phases, the two variables that make the hydromechanical coupling should be considered; the intrinsic pressure of the liquid P and the intrinsic velocity of the solid V_s, which is determined from the deformation of the solid matrix. The mass conservation equations for each phase solid are

$$\underline{\text{Solid}}: \ \frac{\partial \langle \rho_s \rangle}{\partial t} + \vec{\nabla} \cdot [\langle \rho_s \rangle \langle \vec{V}_s \rangle^s] = 0 \tag{4}$$

$$\underline{\text{Liquid}}: \ \frac{\partial \langle \rho_l \rangle}{\partial t} + \vec{\nabla} \cdot [\langle \rho_l \rangle \langle \vec{V}_l \rangle^l] = 0. \tag{5}$$

According to Darcy's Law, one can write the equation of the momentum of the liquid for a deformable medium as follows [37]:

$$\langle \vec{V}_l \rangle^l - \langle \vec{V}_s \rangle^s = -\frac{\overline{\overline{k}}}{\varepsilon_l \mu_l} (\vec{\nabla} \cdot \langle P \rangle^l - \langle \rho_l \rangle^l \vec{g}) = 0. \tag{6}$$

In the above equation, $\overline{\overline{k}}$ is the average permeability tensor.

The conservation equation of the mass of the liquid becomes

$$\frac{\partial \langle \rho_l \rangle}{\partial t} + \vec{\nabla} \cdot \left[\langle \rho_l \rangle \left(\langle \vec{V}_s \rangle^s - \frac{\overline{\overline{k}}}{\varepsilon_l \mu_l} (\vec{\nabla} \cdot \langle P \rangle^l - \langle \rho_l \rangle^l \vec{g}) \right) \right] = 0. \tag{7}$$

The conservation equation of the mass of the liquid, according to the compressibility of the liquid and its volume fraction considering that the effect of the gravity is negligible, is

$$\varepsilon \chi \frac{\partial \langle \rho_l \rangle^l}{\partial t} + \frac{\partial \varepsilon_l}{\partial t} + \frac{1}{\langle \rho_l \rangle^l} \vec{\nabla} \cdot \left[\langle \rho_l \rangle^l \left(\varepsilon_l \langle \vec{V}_s \rangle^s - \frac{\overline{\overline{k}}}{\mu_l} \vec{\nabla} \cdot \langle P \rangle^l \right) \right] = 0. \tag{8}$$

Finally, the conservation equation of the liquid mass is written in the form

$$\varepsilon_l \chi \left[\frac{\partial \langle P_l \rangle^l}{\partial t} + \left(\langle \vec{V}_s \rangle^s - \frac{\overline{\overline{k}}}{\varepsilon_l \mu_l} \vec{\nabla} \cdot \langle P_l \rangle^l \right) \cdot \vec{\nabla} \cdot \langle P_l \rangle^l \right] + \frac{\partial \varepsilon_l}{\partial t} + \vec{\nabla} \cdot \left[\varepsilon_l \langle \vec{V}_s \rangle^s - \frac{\overline{\overline{k}}}{\mu_l} \vec{\nabla} \cdot \langle P \rangle^l \right] = 0. \tag{9}$$

In the conservation equation of the liquid mass, two super imposed effects that will contribute to the transfer of the liquid mass are:

- A term of liquid mass transport following Darcy's law.
- A term of pressure transport.

Taking into consideration the relationship between the bulk density and the intrinsic density with an incompressible solid matrix, the solid mass conservation equation (4) is written as

$$\frac{\partial \varepsilon_s}{\partial t} + \vec{\nabla} \cdot [\varepsilon_s \langle \vec{V}_s \rangle^s] = 0. \tag{10}$$

The mass conservation equation is obtained by the combination of the liquid and solid conservation equations as follows:

$$\varepsilon_l \chi \left[\frac{\partial \langle P_l \rangle^l}{\partial t} + \left(\langle \vec{V}_s \rangle^s - \frac{\overline{\overline{k}}}{\varepsilon_l \mu_l} \vec{\nabla} \cdot \langle P_l \rangle^l \right) \cdot \vec{\nabla} \cdot \langle P_l \rangle^l \right] + \vec{\nabla} \cdot \left[\langle \vec{V}_s \rangle^s - \frac{\overline{\overline{k}}}{\mu_l} \vec{\nabla} \cdot \langle P_l \rangle^l \right] = 0. \tag{11}$$

3.2. *Momentum equation*

Taking into account the hypothesis of a quasi-static environment allows the neglecting of inertia terms. The effect of gravity is neglected on the displacement of the solid. These hypotheses lead to writing the equation of conservation of the momentum of the medium under its skeleton of static equilibrium or stress equilibrium as follows [42]:

$$\vec{\nabla}\cdot\overline{\overline{\sigma}} = \vec{\nabla}(\varepsilon_s\overline{\overline{\sigma_s}} - \varepsilon_l\langle P_l\rangle^l\,\overline{\overline{I}}) = 0. \tag{12}$$

The stress analyzes are possible if the principle of effective stresses proposed by Gustavo [40] is applied. The obtaining of this effective constraint is carried out starting from a balance of forces on the solid network as follows:

$$\overline{\overline{\sigma}} = \overline{\overline{\sigma_{\text{eff}}}} - \langle P_l\rangle^l\,\overline{\overline{I}}. \tag{13}$$

When the behavior is elastic, Hooke's law expresses the relationship between the effective constraint and the displacement of the solid network as follows:

$$\overline{\overline{\sigma_{\text{eff}}}} = E\cdot\overline{\overline{\varepsilon}}. \tag{14}$$

The writing of the motion conservation equation during the drying of a saturated and deformable porous medium in its static equilibrium form is

$$\vec{\nabla}\cdot\overline{\overline{\sigma}} = \vec{\nabla}(E\cdot\overline{\overline{\varepsilon}}) - \vec{\nabla}\cdot(\langle P_l\rangle^l\,\overline{\overline{I}}) = 0. \tag{15}$$

The above equation meets the rheology of the solid matrix at liquid pressure. The tensor of deformations and the speed of shrinkage are obtained by solving this equation.

The total strain tensor [39] is the sum of the strain tensor related to the mechanical behavior of the material and the strain tensor related to isotropic shrinkage (not producing stress in the medium). By definition, the deformation tensor of Green–Lagrange as a function of the deformation rate of the solid is written as

$$\overline{\overline{\varepsilon}} = 0.5(\vec{\nabla}\langle\vec{V}_s\rangle^s\,\mathrm{d}t + T\vec{\nabla}\langle\vec{V}_s\rangle^s\,\mathrm{d}t + T\vec{\nabla}\langle\vec{V}_s\rangle^s\,\mathrm{d}t\vec{\nabla}\langle\vec{V}_s\rangle^s\,\mathrm{d}t). \tag{16}$$

3.3. *Energy conservation equations*

In the study of porous media, the local thermal equilibrium hypothesis is frequently used. The meaning of the hypothesis is that the macroscopic temperatures of the phases are sufficiently close to be able to use a single macroscopic temperature, which is the average temperature in the REV(T). The conservation equation of energy, taking into account the hypothesis of local thermal equilibrium, in a porous two-phase deformable medium ($\langle T\rangle = \langle T_s\rangle = \langle T_l\rangle$), is written as

$$\langle\rho C_p\rangle\frac{\partial\langle T\rangle}{\partial t} + [(\rho C_p)_l\langle\vec{V}_l\rangle + (\rho C_p)_s\langle\vec{V}_s\rangle]\vec{\nabla}\langle T\rangle = \vec{\nabla}\cdot(\overline{\overline{\lambda}}_{\text{eff}}\vec{\nabla}\langle T\rangle), \tag{17}$$

where λ_{eff} is the effective conduction coefficient which depends on the intrinsic thermal characteristics of each phase and their geometric distribution.

Using the following equalities and neglecting the effect of gravity in the expression of Darcy's law, the conservation equation of energy becomes

- $\langle\vec{V}_l\rangle = \varepsilon_l\langle\vec{V}_l\rangle^l; \quad \langle\vec{V}_s\rangle = \varepsilon_s\langle\vec{V}_s\rangle^s$ (18)
- $\langle\rho C_p\rangle = \varepsilon_l\langle\rho C_p\rangle_l + \varepsilon_s\langle\rho C_p\rangle_s$ (19)

$$\langle\rho C_p\rangle\frac{\partial\langle T\rangle}{\partial t} + \left[\langle\rho C_p\rangle\langle\vec{V}_s\rangle^s - (\rho C_p)_l\frac{\overline{\overline{k}}}{\mu_l}\vec{\nabla}\cdot\langle P_l\rangle^l\right]\vec{\nabla}\langle T\rangle = \vec{\nabla}\cdot(\overline{\overline{\lambda}}_{\text{eff}}\vec{\nabla}\langle T\rangle). \tag{20}$$

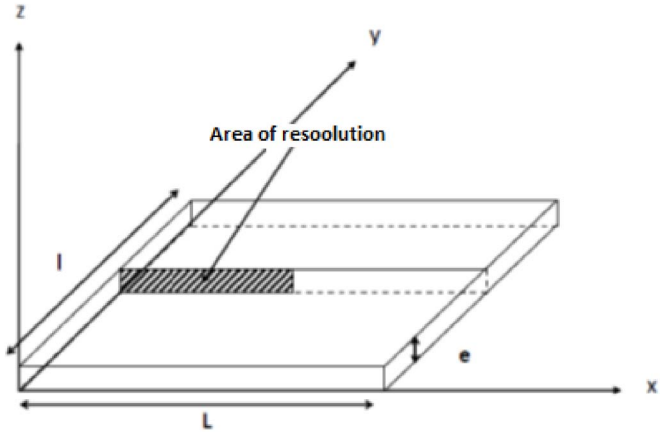

Figure 3. Computed domain.

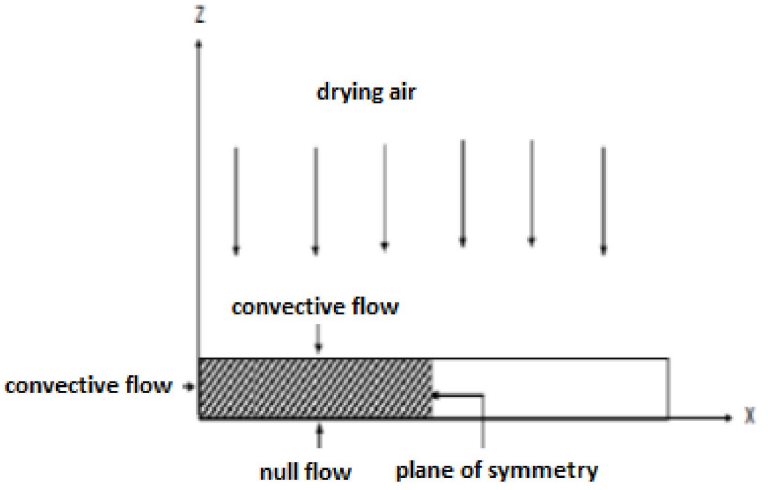

Figure 4. Area of the sample and the boundary conditions.

4. Simulation of transport phenomena

The conservation equations with the variables (ε, P, V, and T), are solved to obtain the effect of the thermo-hydro-mechanical coupling during the process of convective drying by the hot air of a bovine leather coupon of dimension ($L = 16$ cm, $l = 14$ cm, $e = 1.2$ mm), as shown in Figure 3.

4.1. *Full equations' system*

The bidirectional configuration of the tested sample is shown in Figure 4. Two exchange and two symmetric surfaces bound the quarter of the sample, and the governing equations are (11), (15), (16), and (18).

The system of equations is solved in the (x, z) plane as shown in Figure 4. The initial conditions of the sample state are at a uniform temperature and humidity with atmospheric pressure and zero stress. Mathematically, these conditions are expressed as follows:

$$T = T_o, \quad X = X_o, \quad P = P_o, \quad \text{and} \quad \sigma_{ij} = 0. \tag{21}$$

4.2. *Boundary conditions*

At the sample's higher face

Water transfer:

$$\left[\rho_l \frac{K}{\mu_l}\vec{\nabla}\langle P_l\rangle\right]\cdot\vec{n} = K_{m,L}\frac{M_v}{R}\left(\frac{a_w(X,T)*P_{\text{sat}}(T_{\text{surf}})}{T_{\text{surf}}} - \frac{HR*P_{\text{sat}}(T_a)}{T_a}\right). \tag{22}$$

Heat transfer equation:

$$\left[-\lambda\frac{\partial\langle T\rangle}{\partial n}\right]_{\text{surf}} + \left[\langle\rho C_p\rangle\langle\vec{V}_s\rangle^s - (\rho C_p)_l\frac{\overline{\overline{k}}}{\mu_l}\vec{\nabla}\cdot\langle P_l\rangle^l\right]\langle T\rangle\cdot\vec{n} = h_L(T_{\text{surf}}-T_a) - \Delta h_{\text{vap}}\left[\rho_l\frac{K}{\mu_l}\vec{\nabla}\langle P_l\rangle\right]\cdot\vec{n}. \tag{23}$$

The coefficients of heat and mass transfer are evaluated by Nusselt number empirical correlations and Sherwood number [42].

$$h_L = \frac{\lambda_a}{L} * [0.667 Re_L^{0.5} Pr^{0.33}] \tag{24}$$

$$K_{m,L} = \frac{D_a}{L} * [0.667 {Re_L}^{0.5} Sc^{0.33}]. \tag{25}$$

Sample's lateral face:

Water transfer

$$\left[\rho_l\frac{K}{\mu_l}\vec{\nabla}P_l\right]\cdot\vec{n} = K_{m,e}\frac{M_v}{R}\left(\frac{a_w(X,T)*P_{\text{sat}}(T_{\text{thickness}})}{T_{\text{thickness}}} - \frac{HR*P_{\text{sat}}(T_a)}{T_a}\right). \tag{26}$$

Heat transfer:

$$\left[-\lambda\frac{\partial\langle T\rangle}{\partial n}\right]_{\text{surf}} + \left[\langle\rho C_p\rangle\langle\vec{V}_s\rangle^s - (\rho C_p)_l\frac{\overline{\overline{k}}}{\mu_l}\vec{\nabla}\cdot\langle P_l\rangle^l\right]\langle T\rangle\cdot\vec{n} = h_e(T_P-T_a) - \Delta h_{\text{vap}}\left[\rho_l\frac{K}{\mu_l}\vec{\nabla}\langle P_l\rangle\right]\cdot\vec{n} \tag{27}$$

$$h_e = \frac{\lambda_a}{e} * [0.628 {Re_e}^{0.5} Pr^{0.33}] \tag{28}$$

$$K_{m,e} = \frac{D_a}{e} * [0.628 {Re_e}^{0.5} Sc^{0.33}] \tag{29}$$

symmetry plane

$$\left(\rho_l\frac{K}{\mu_l}\vec{\nabla}P_l\right)\cdot\vec{n} = 0 \tag{30}$$

$$\lambda\left.\frac{\partial T}{\partial n}\right|_{\text{surf}} = 0. \tag{31}$$

It is assumed the product's surface has no external forces applied to it. The boundary condition for the conservation of momentum is

$$\sigma_{ij,\text{surf}} = 0. \tag{32}$$

Moreover, it was assumed that, the solid displacement in the z (vertical) direction at the surface in contact with the shelf ($z = 0$) was considered nil ($V_z = 0$). Besides, the solid displacement in x (horizontal) direction at the symmetry plane ($x = 0$) were considered equally nil.

4.3. *Thermophysical properties of leather*

The main thermophysical properties of leather were collected from our previously published works Benmakhlouf Naima; the model parameters of DENT depend on the temperature and can correctly describe the pace of the different isotherms [27, 28]. The properties are presented in Table 2.

Table 2. Thermophysical properties of leather

Desorption isotherm: DENT model	$X_{eq} = \dfrac{Hr}{A \cdot Hr^2 + B \cdot Hr + C}$
Leather density	$\rho_s = 1221$ kg·m^{-3}
Thermal conductivity	$\lambda = 0.048$ W·m^{-1}·K^{-1}
Young modulus	$E = 22.10^6$ Pa [30]
Permeability	$K = 10^{-13}$ m^2 [29]

4.4. *Numerical implementation of the model equations*

The equations were solved numerically in 2D using a commercial solver (COMSOL Multiphysics, version 3.5a) working with the finite element method. This solution method can follow the change in the geometry of the material during drying. Besides, it is recommended for deformable martial, because it has the advantage of following the material's geometry variation during drying.

Due to the symmetry of the problem, the numerical computation is limited to a rectangular 2D domain representative of the leather sample. The solution area has been meshed with very refined triangular elements toward the borders. The direct solver (UMFPACK) was used for the numerical resolution of the equations implemented on the code.

5. Results and discussion

5.1. *Model validation*

The model validation is performed by comparing the transient variation of the average moisture content of the leather coupon obtained from numerical simulation of the liquid volume fraction to the experimental data, as shown in Figure 5. Indeed, the results of the numerical simulation are relatively in good agreement with those of the experiments. The observed discrepancies between the two results are mainly from the non-precise evaluation of the various parameters of the material. These discrepancies are due to the permeability and Young's modulus which are key parameters of the simulation, the hypothesis of a medium remaining saturated, and the accuracy of the initial and boundary conditions.

The model developed has been also validated by reference to the variation of the temperature at the heart of the leather coupon at different thicknesses. Experimental evolutions of the temperature at the center of the product, as a function of time, are presented in Figure 6. From the results presented, the agreement is reasonable between the experimental and simulated curves. The maximum relative difference between the experimental and simulated drying time does not exceed 10% for all drying conditions, which is satisfactory, given the complexity of the measurements and the means used. Temperature measurements will be more accurate if they are measured using optical fibers or remotely using infra-red thermometers.

5.2. *Hydrothermal and rheological state simulation*

The liquid pressure variation in the leather coupon center changes is presented in Figure 7. A high drop in the liquid's pressure is observed. On the medium's surface, the importance of the surface tension requires high values of the capillary pressure, which justifies the liquid's pressure significant negative values. Moreover, the values of the liquid's pressure mainly depend on the

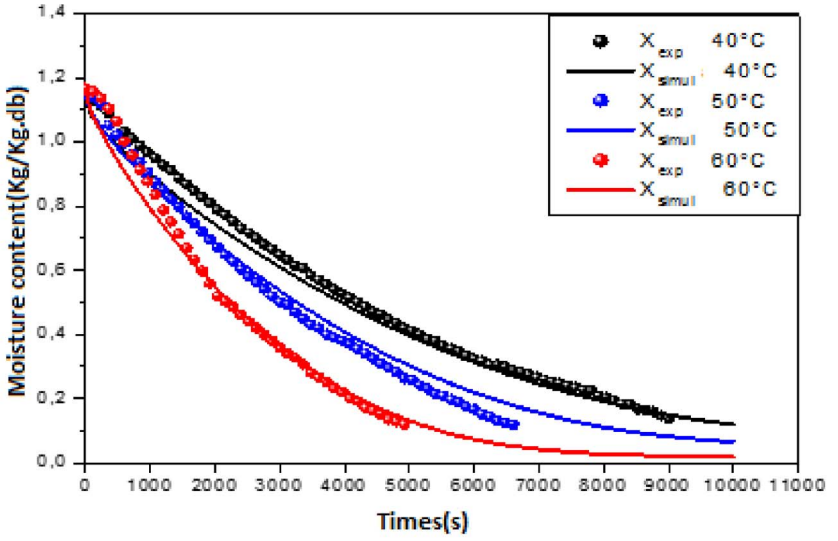

Figure 5. Experimental and simulated average moisture. Content of the leather coupon versus time (RH = 15%, $v = 1\ \mathrm{m{\cdot}s^{-1}}$).

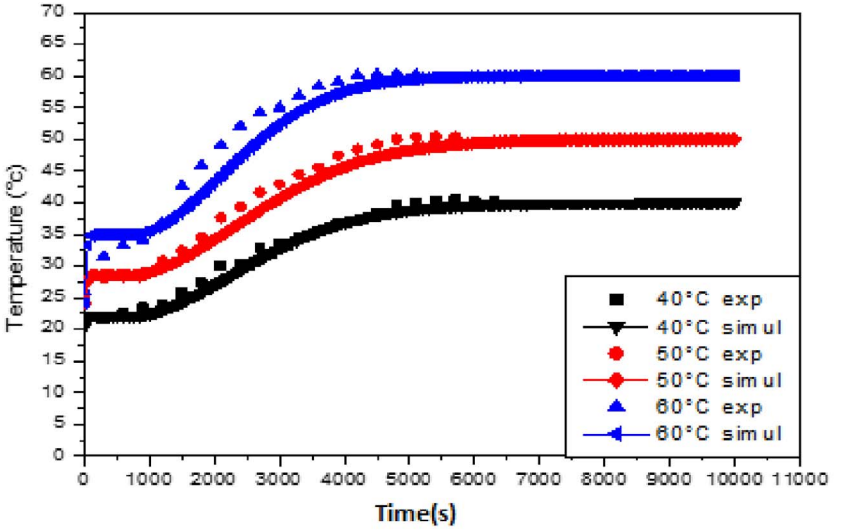

Figure 6. The center temperature of the leather coupon versus time (RH = 15%, $v = 1\ \mathrm{m{\cdot}s^{-1}}$).

rheological parameters, which are expressed in the equation of the rheological behavior of the product, and also on the liquid permeability of the medium, which is expressed in the equation of water transfer.

Figure 8 shows the transient variation of the liquid volume fraction for the different drying scenarios. The results show that the drying is more accentuated with the drying air temperature. The drying air temperature affects the properties of the medium and the boundary conditions of the model (the transfer coefficients and the saturation vapor pressure). The observed shape of

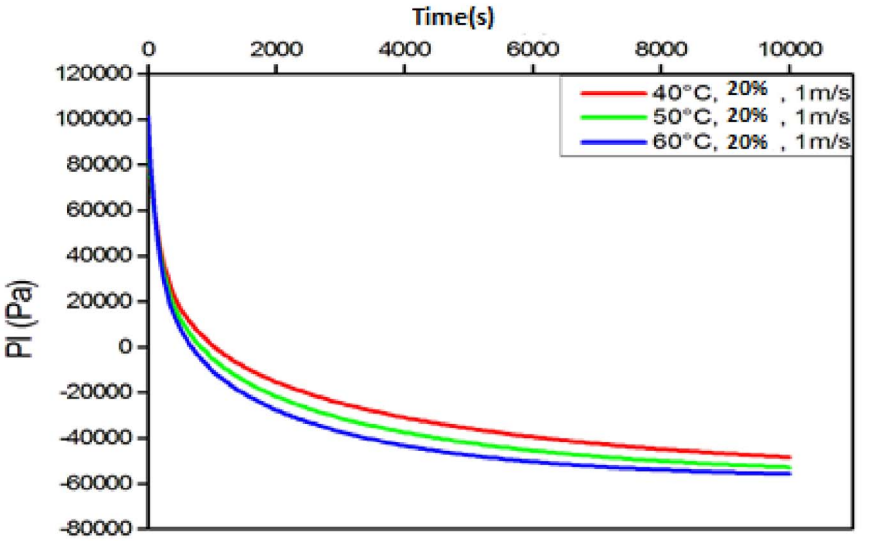

Figure 7. The liquid pressure in the center of the leather coupon.

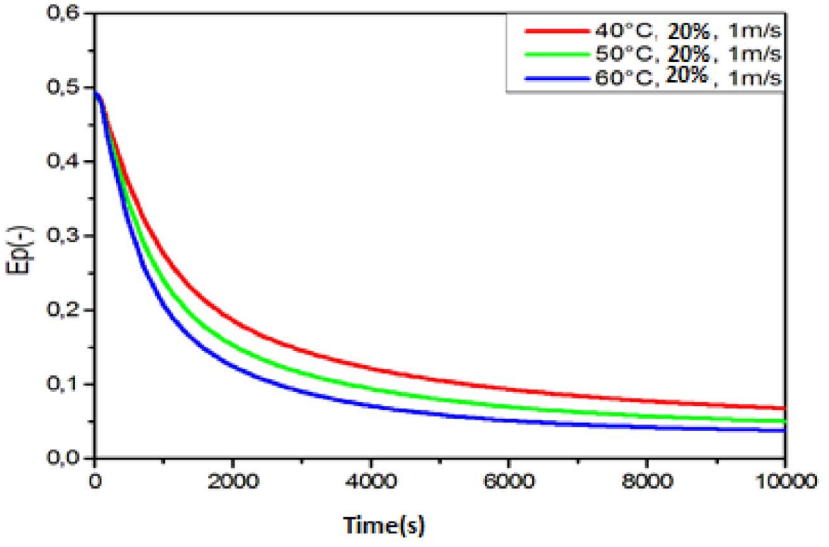

Figure 8. The liquid fraction in the center of the leather coupon.

the liquid volume fraction curves shows that moisture transport is convective in nature and that the flow of water is easy within the material. That is why there are no very important gradients.

Figure 9 shows the transient distribution of temperature profiles. It is noted that the thermal gradient is small and is only significant at the beginning of drying, given the small thickness of the sample.

A rise in temperature corresponding to the set phase is observed. Then, a stabilization corresponding to the phase of drying at a constant speed is developed, and the energy brought to the medium is released largely for the flow of steam leaving the surface. The temperature increases

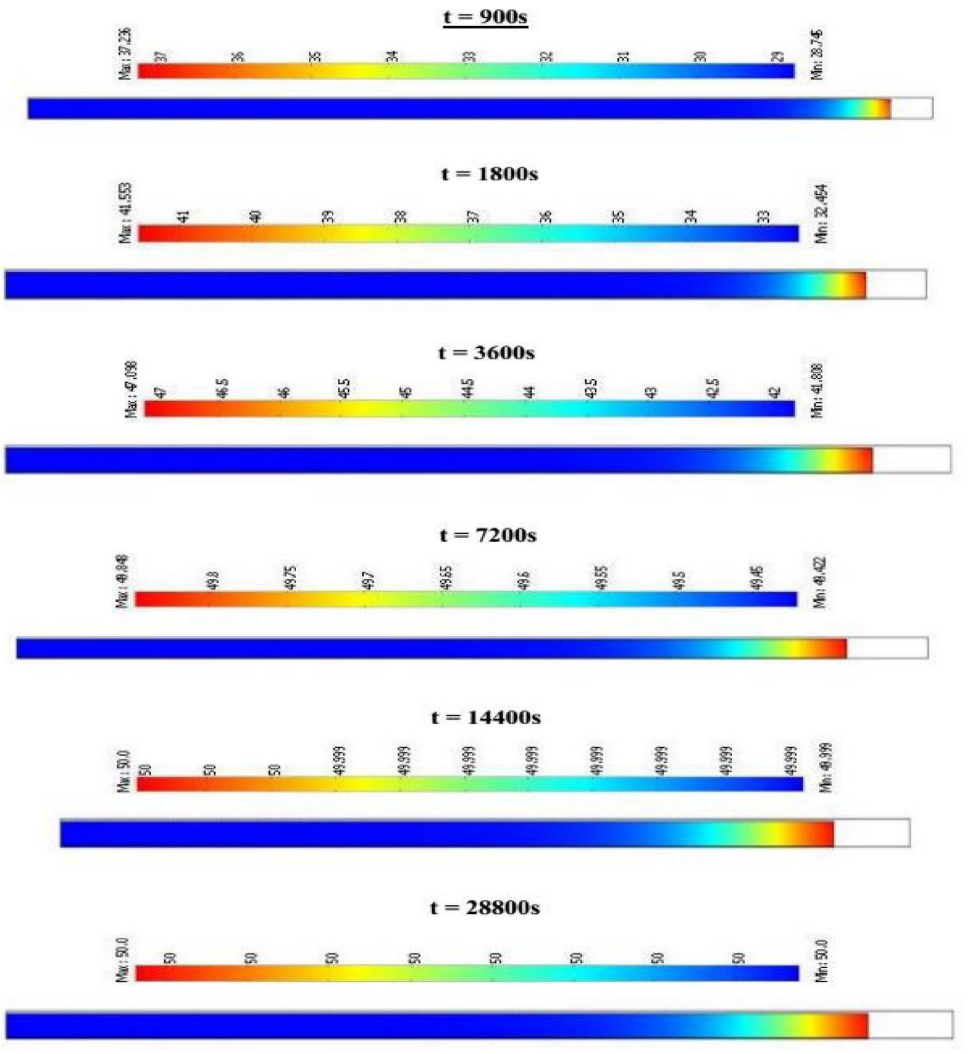

Figure 9. Temperature profiles during drying (50 °C, RH = 20%, $v = 1$ m·s^{-1}).

because of the drop in the mass flow rate at the surface and the product reaches a temperature close to that of the drying air. Figure 10 shows the profiles of the liquid volume fraction (proportional to the water content of the medium) for different drying times. The fraction of liquid volume decreases as a function of time from its initial value of 0.55 to its average equilibrium value of 0.15. Since the water gradient is high at the upper surface, a decrease in the liquid fraction is noted. The high gradient increases the diffusion of moisture in this region. At the end of the drying process, the content of liquid water approaches equilibrium with the surrounding air and the gradient of the liquid water diminishes.

Once the mechanical stresses are known, the mechanical damage that may occur during drying to release the mechanical energy stored in the medium could be avoided. The curves of the transient behavior of the mechanical stress at the heart of the product for three drying scenarios are presented in Figure 11.

The negative and positive stress values designate compression and traction, respectively. At the beginning of drying, it is observed that the level of stress rapidly rises because the

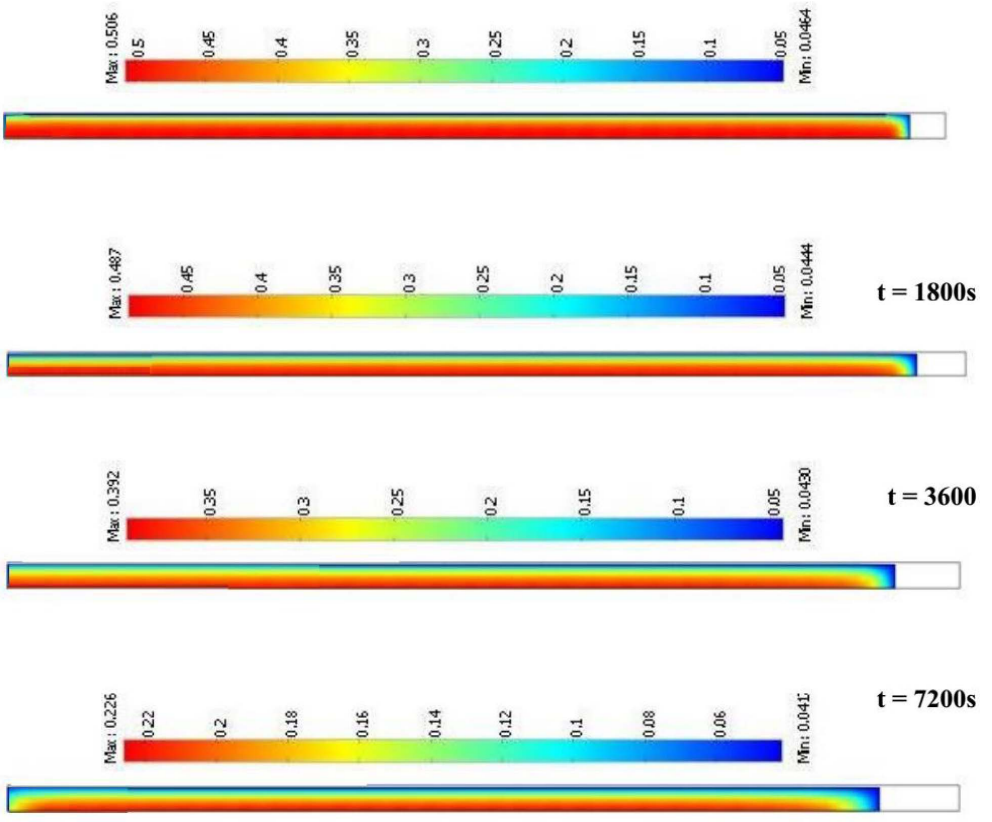

Figure 10. Simulation of the liquid fraction during drying.

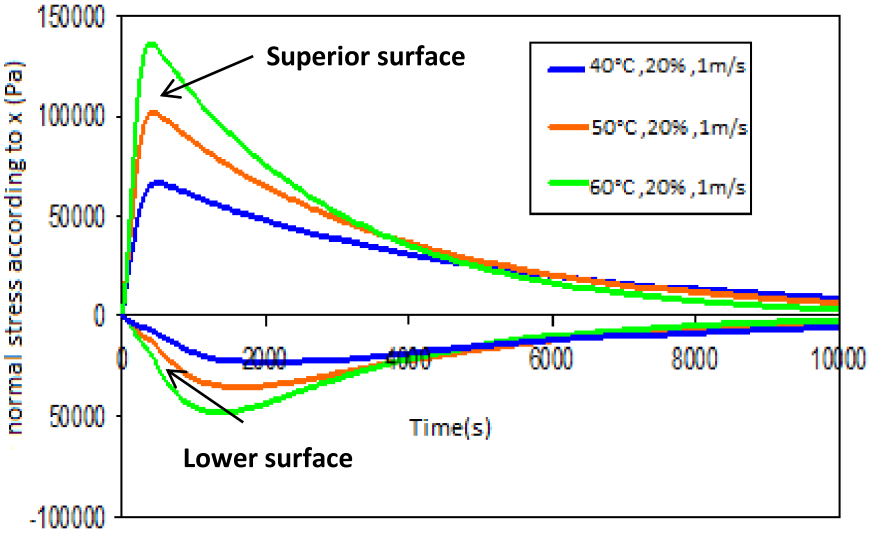

Figure 11. Normal stress on x, on the upper and lower surface.

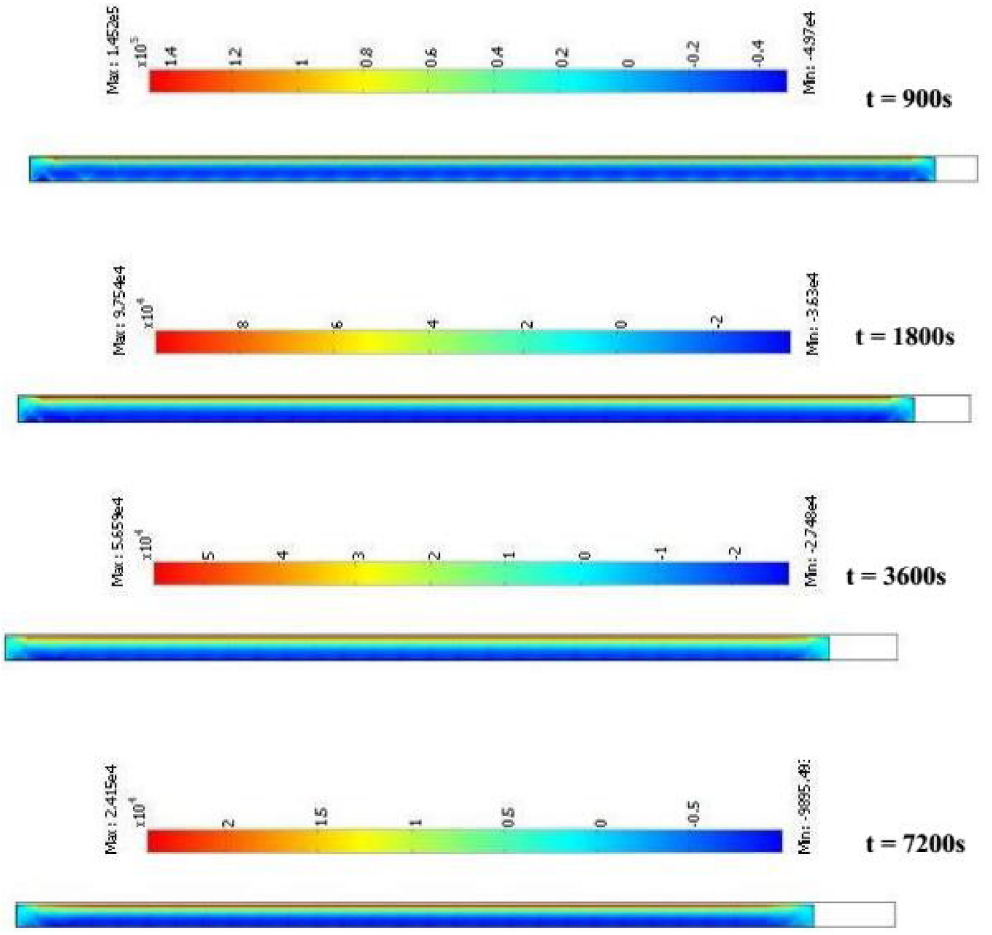

Figure 12. Simulation of the normal stress according to x during drying.

water content gradient increases. The gradient then passes through a maximum, which corresponds to the beginning of the phase at decreasing speed and, at a later stage, it decreases until it is canceled. These results are supported by already published results [43–46]. The damage of the sample is more likely to occur at the beginning of the drying in the time interval of 300–400 s.

According to these simulations, the sample's face, which is exposed to the drying air, has the strongest stress; therefore, the sample's face is at a high risk of cracking. Since the lower layers of the sample are in a compression state, the surface crack could not be extended to them. It is also observed that the risk of damage to the sample corresponding to the maximum level of the stress is higher for the highest drying temperature. The peak for the three thicknesses of leather is reached for normal stresses equal is between the interval to 60,000 and 140,000 MPa at around 10,000 s.

Figure 12 shows the profiles of the normal stress according to x for different drying times. Note that the level of stress is greater at the surface exposed to drying air. The risk of damage is then more likely over the entire upper surface of the sample. Besides, the tensile stress at the peripheral layer of the sample (positive values) is compensated by the compression stress inside (negative values), which ensures the equilibrium of the sample and thus confirms the result of Figure 11.

The profiles also give us an idea about the withdrawal of the sample during drying through the displacements of the surface.

6. Conclusion

A study of a 2D transitory model of a drying process to describe the physical phenomena in deformable materials was developed. The coupled liquid and heat transfer governing equations with their corresponding initial and boundary conditions were numerically implemented and solved using COMSOL Multiphysics software. Experimental data of water content, temperature, and geometric shape were used to validate the model. Different simulation results have been interpreted and explored in terms of mechanical deformation of the leather sample, toward the optimization of the process. For the same drying conditions, the internal pressure levels of the vapor phase evaluated by numerical simulations were compared to the maximum stresses determined experimentally through the mechanical tests to define the optimal leather drying conditions. The results showed that the higher the level of internal pressure, the lower the maximum resistance of the dried leather. A good agreement was established between the experimentally obtained results and the simulation at the conditions of 40 °C, RH 20% and 60 °C, RH 20%. It was found that the optimum normal stresses were estimated and the risk of crack appeared during the decreasing drying rate period.

For further study, we foresee a continuation of this work from an experimental and numerical point of view, considering certain points like the treatment of the anisotropic appearance of leather in the case of a three-dimensional hydro-thermomechanical simulation with more complex mechanical behaviors (viscoelastic, elastoviscoplastic, etc.).

Nomenclature

a_w	Water activity
C	Concentration
D	Moisture diffusivity ($m^2 \cdot s^{-1}$)
d	Diameter (m)
h	Coefficient of heat transfer ($W \cdot m^{-2} \cdot k^{-1}$)
RH	Relative Humidity (%)
K_m	Coefficient of mass transfer ($m \cdot s^{-1}$)
M	Mass (kg)
P	Pressure (Pa)
Pr	Prandtl number
Re	Reynolds number
R	Ideal gas constant ($J \cdot mol^{-1} \cdot K^{-1}$)
t	Time (s)
T	Temperature (°C)
Sc	Schmidt number
v	Velocity ($m \cdot s^{-1}$)
V	Volume (m^3)
X	Moisture content (kg water per kg dry air)

Greek letters

ρ	Density ($kg \cdot m^{-3}$)
λ	Thermal conductivity ($W \cdot m^{-1} \cdot K^{-1}$)
μ	Dynamic viscosity ($kg \cdot m^{-1} \cdot s^{-1}$)

Subscripts

0	Initial
A	Air
eq	Equilibrium
exp	Experimental
simul	Simulation
l	Liquid
s	Solid
v	Vapor

Acknowledgments

The authors would like to thank the National Agency for the Promotion of Scientific Research (ANPR) thesis research and innovations are performed within the framework of the MOBIDOC thesis, financed by the EU under the program PASRI. This research was supported by Tannerie Megisserie du Maghreb industry as the research partner. The authors would gratefully acknowledge the financial support received from them and thank all the team of the TMM industry and especially M. Hechmi Khedira, the management environment responsible in the TMM industry.

References

[1] S. J. Kowalski, K. Rajewska, A. Rybicki, "Mechanical effects in saturated capillary-porous materials during convective and microwave drying", *Dry. Technol.* **22** (2004), no. 10, p. 2291-2308.
[2] R. A. Lemus-Mondaca, C. E. Zambra, A. Vega-Gálvez, N. O. Moraga, "Coupled 3D heat and mass transfer model for numerical analysis of drying process in papaya slices", *J. Food Eng.* **116** (2013), no. 1, p. 109-117.
[3] D. Mihoubi, F. Zagrouba, J. Vaxelaire, A. Bellagi, M. Roques, "Transfer phenomena during the drying of a shrinkable product: Modeling and simulation", *Dry. Technol.* **22** (2004), no. 1–2, p. 91-109.
[4] G. K. Vagenas, D. Marinos-Kouris, G. D. Saravacos, "An analysis of mass transfer in air-drying of food", *Dry. Technol.* **19** (1990), no. 2, p. 323-342.
[5] C. T. Kiranoudis, Z. B. Maroulis, D. Marinos-Kouris, "Heat and mass transfer model building in drying with multi response data", *Int. J. Heat Mass Transfer* **38** (1995), no. 3, p. 463-480.
[6] N. Wang, J. G. Brennan, "A mathematical model of simultaneous heat and moisture transfer during drying of potato", *J. Food Eng.* **24** (1996), p. 47-60.
[7] A. J. Ketelaars, "Drying deformable media", PhD Thesis, University of Technology, The Netherlands, 1992.
[8] M. N. A. Hawlader, J. C. Ho, Q. Zang, "A mathematical model for drying of shrinkable materials", *Dry. Technol.* **17** (1999), no. 1–2, p. 27-47.
[9] P. Perré, B. K. May, "A numerical drying model that accounts for the coupling between transfers and solid mechanics. Case of highly deformable products", *Dry. Technol.* **19** (2001), no. 8, p. 1629-1643.
[10] H. Yang, N. Sakai, M. Watanable, "Drying model with non-isotropic shrinkage deformation undergoing simultaneous heat and mass transfer", *Dry. Technol.* **19** (2001), no. 7, p. 1441-1460.
[11] B. K. May, P. Perré, "The importance of considering exchange surface area reduction to exhibit a constant drying flux period in food stuffs", *J. Food Eng.* **54** (2005), p. 271-282.
[12] W. P. Silva, J. W. Precker, D. D. P. S. Silva, C. D. P. S. Silva, A. G. Barbosa de Lima, "Numerical simulation of diffusive processes in solids of revolution via the finite volume method and generalized coordinates", *Int. J. Heat Mass Transfer* **52** (2009), p. 4976-4985.
[13] S. Chemkhi, F. Zagrouba, A. Bellagi, "Mathematical model for drying of highly shrinkable media", *Dry. Technol.* **22** (2004), no. 5, p. 1023-1039.
[14] D. Mihoubi, A. Bellagi, "Stress generated during drying of saturated porous media", *Transp. Porous Media* **80** (2009), no. 3, p. 519-536.
[15] D. Mihoubi, A. Bellagi, "Two-dimensional heat and mass transfer during drying of deformable media", *Appl. Math. Model.* **32** (2008), no. 3, p. 303-314.
[16] F. P. Incropera, D. P. DeWitt, *Fundamentals of Heat and Mass Transfer*, 5th ed., John Wiley & Sons Inc, New York, 2002, 698 p.
[17] A. A. J. Ketelaars, "Drying deformable: media kinetics, shrinkage and stresses", *Dry. Technol.* **12** (1994), no. 4, p. 983-987.

[18] C. Moyne, N. Kechaou, P. J. Do AmralSobral, M. Roques, A. Cairault, H. Bizot, "Mechanism of water transport in drying of gels", *Int. Chem. Eng.* **34** (1994), no. 3, p. 360-369.
[19] B. A. Manel, D. Mihoubi, S. Jalila, B. Ahmed, "Strain stress formation during stationary and intermittent drying of deformable media", *Dry. Technol.* **32** (2014), no. 10, p. 1245-1255.
[20] B. A. Manel, S. Jalila, M. Daoued, B. Ahmed, "Multiphase thermo-hydro-mechanical model for concrete under drying at high temperatures", *Dry. Technol.* **33** (2015), no. 2, p. 143-152.
[21] G. Johann, M. De Menezes, N. Curvelo Pereira, E. A. da Silva, "Comparing models to Neumann and Dirichlet conditions in grape seed drying", *Appl. Therm. Eng.* **93** (2016), p. 865-871.
[22] C.-K. Liu, C. P. Latona, J. Lee, "Drying leather with vacuum and toggling sequentiaLLy", *J. Am. Leather Chem. Assoc.* **106** (2011), p. 76-82.
[23] J. Zhang, C. Zhang, J. Wu, W. Chen, "Advantages of utilizing microwave in soft leather drying", *Leather Footwear J.* **17** (2017), p. 81-86.
[24] N. Proietti, V. Di Tullio, C. Carsote, E. Badea, "C solid-state NMR complemented by ATR-FTIR and micro-DSC to study modern collagen-based material and historical leather", *Magn. Reson. Chem.* **58** (2020), no. 9, p. 840-859.
[25] A. Ershad-Langroudia, A. Mirmontahaia, R. Vahidzadeh, "Viscoelastic behavior of treated historical leather with nanocomposite", in *Proceedings of the 4th International Conference on Nanostructures (ICNS4), Kish Island, Islamic Republic of Iran*, March 12–14, 2012, *J. Am. Leather Chem. Assoc.* **108** (2013), no. 12.
[26] S. Kabeer, G. Attenburrow, P. Picton, M. Wilson, "Development of an image analysis technique for measurement of Poisson's ratio for viscoelastic materials: application to leather", *J. Mater. Sci.* **48** (2013), p. 744-749.
[27] N. Benmakhlouf, S. Azzouz, H. Khedhira *et al.*, "Moisture sorption isotherms of leather", *J. Soc. Leather Technol. Chem.* **100** (2016), no. 2, p. 77-83.
[28] N. Benmakhlouf, S. Azzouz, J. M. Cabrera *et al.*, "Controlling mechanisms of moisture diffusion in convective drying of leather", *J. Heat Mass Transfer* **53** (2017), p. 1237-1245.
[29] R. Younsi, "Simulation numerique du transfertde chaleur et de masse en milieuxfluides et poreux", PhD Thesis, Université des Sciences et de la Technologie Houari Boumediene, 2007.
[30] Z. Li, D. Paudecerf, J. Yang, "Mechanical behaviour of natural cowleather in tension", *Acta Mech. Solid Sin.* **22** (2009), no. 1, p. 37-44.
[31] S. Chemkhi, F. Zagrouba, A. Bellagi, "Mathematical model for drying of highly shrinkage media", *Dry. Technol.* **22** (2004), no. 5, p. 1023-1039.
[32] J. Monzd-Cabrera, A. Diaz-MorcilloJos, M. Catalfi-Civeraet, E. de los Reyes, "Heat flux and heat generation characterisation in a wet-laminar body in microwave-assisted drying: an application to microwave drying of leather", *Int. Comm. Heat Mass Transfer* **27** (2000), no. 8, p. 1101-1110.
[33] A. K. Haghi, "A mathematical model of the drying process", *Acta Polytech. J.* **41** (2001), no. 3, p. 20-23.
[34] A. K. Haghi, "Simultaneous moisture and heat transfer in porous systems", *J. Comput. Appl. Mech.* **2** (2001), p. 195-204.
[35] A. K. Haghi, "Mechanism of heat and mass transfer in moist porous materials", *J. Teknol.* **36** (2002), p. 1-14.
[36] A. K. Haghi, "Factors effecting water-vapor transport through fibers", *Theor. Appl. Mech.* **30** (2003), no. 4, p. 277-309.
[37] S. Whitaker, "Simultaneous heat mass and momentum transfer in porous media a theory of drying", *Adv. Heat Transfer* **13** (1977), p. 119-203.
[38] S. Sandoval-Torres, J. Rodríguez-Ramírez, L. L. Méndez-Lagunas, "Modeling plain vacuum drying by considering a dynamic capillary pressure", *Chem. Biochem. Eng.* **25** (2011), no. 3, p. 327-334.
[39] W. Jomaa, "Séchage de matériaux fortement déformables : Pprise en compte de la vitesse de retrait", PhD Thesis, Université de Bordeaux I, 1991.
[40] S. Gustavo, "Modélisation du séchage d'un milieu poreux saturé déformable : Prise en compte de la pression du Liquide", PhD Thesis, École Nationale d'Art et des métiers centre de Bordeaux, 2006.
[41] B. Collignon, "Séchage des bétons réfractaires : expérimentation, modélisation et influence d'un ajout de fibres polymère", PhD Thesis, Institut Nationale Polytechnique de Laurraine, 2009.
[42] F. D. Incropera, D. P. Dewitt, *Fundamentals of Heat and Mass Transfer*, 4th ed., John Wiley & Sons, 1996.
[43] G. Almeida, J. P. Lancha, F. Pierre, J. Casalinho, P. Perré, "Physical behavior of highly deformable products during convective drying assessed by a new experimental device", *Dry. Technol.* **35** (2017), no. 8, p. 906-917.
[44] B. A. Manel, D. Mihoubi, S. Jalila, B. Ahmed, "Strain–stress formation during stationary and intermittent drying of deformable media", *Dry. Technol.* **32** (2014), no. 10, p. 1245-1255.
[45] B. A. Manel, S. Jalila, M. Daoued, B. Ahmed, "Multiphase thermo-hydro-mechanical model for concrete under drying at high temperatures", *Dry. Technol.* **33** (2015), no. 2, p. 143-152.
[46] F. Benboudjema, F. Meftah, J.-M. Torrenti, "Interaction between drying, shrinkage, creepand cracking phenomena in concrete", *Eng. Struct.* **27** (2005), no. 2, p. 239-250.